Probing the circumstellar structure of Herbig Ae/Be stars

Jorick S. Vink[1], Janet E. Drew[1], Tim J. Harries[2], René D. Oudmaijer[3]

[1] *Imperial College of Science, Technology and Medicine, Blackett Laboratory, Prince Consort Road, London, SW7 2BZ, UK*
[2] *School of Physics, University of Exeter, Stocker Road, Exeter EX4 4QL, UK*
[3] *The Department of Physics and Astronomy, E C Stoner Building, Leeds, LS2 9JT, UK*

ABSTRACT

We present Hα spectropolarimetry observations of a sample of 23 Herbig Ae/Be stars. A change in the linear polarisation across Hα is detected in a large fraction of the objects, which indicates that the regions around Herbig stars are flattened (disc-like) on small scales. A second outcome of our study is that the spectropolarimetric signatures for the Ae stars differ from those of the Herbig Be stars, with characteristics changing from depolarisation across Hα in the Herbig Be stars, to line polarisations in the Ae group. The frequency of depolarisations detected in the Herbig Be stars (7/12) is particularly interesting as, by analogy to classical Be stars, it may be the best evidence to date that the higher mass Herbig stars are surrounded by flattened structures. For the Herbig Ae stars, 9 out of 11 show a line polarisation effect that can be understood in terms of a compact Hα emission that is itself polarised by a rotating disc-like circumstellar medium. The spectropolarimetric difference between the Herbig Be and Ae stars may be the first indication that there is a transition in the Hertzsprung-Russell Diagram from magnetic accretion at spectral type A to disc accretion at spectral type B. Alternatively, the interior polarised line emission apparent in the Ae stars may be masked in the Herbig Be stars due to their higher levels of Hα emission.

Key words:
stars: formation – stars: pre-main sequence – stars: Herbig Ae/Be – circumstellar matter – techniques: polarimetric

1 INTRODUCTION

Although we seem to understand reasonably well how low mass stars form by cloud collapse and disc accretion, the question of whether high mass stars form in the same way remains completely open. On the one hand, theoretical efforts are being undertaken to realise the formation of high mass stars through disc accretion (e.g. Behrend & Maeder 2001). On the other hand, others perform calculations for the formation of high mass stars by stellar collisions and mergers in a dense cluster environment (e.g. Bonnell, Bate & Zinnecker 1998). These collision scenarios are invoked because high mass star formation through disc accretion encounters the problem that radiation pressure forces on gas and dust may be able to reverse the infall, preventing the formation of stars with masses larger than 10 M$_\odot$ (York & Kruegel 1977).

In addressing the question as to whether accretion discs around high mass stars are present, the intermediate mass (2 − 15 M$_\odot$) pre-main sequence Herbig Ae/Be stars (Herbig

1960) play a crucial role, as these objects are the only higher mass pre-main sequence stars that are visible at optical and infrared wavelengths. Yet, whether or not Herbig Ae/Be stars are embedded in accretion discs has not been determined. Although there is clear-cut evidence for the presence of circumstellar gas and dust (see e.g. Waters & Waelkens 1998), there is no consensus on the *geometry* of this material (see e.g. Pezzuto, Strafella & Lorenzetti 1997 for a summary of conflicting views). Ideally one would like to solve this issue by directly imaging the environments around these objects. Although there are indications that some intermediate mass stars present geometries deviating from spherical symmetry (e.g. Mannings & Sargent 1997; Grady et al. 1999; Shepherd, Claussen & Kurtz 2001), the conclusions reached are sometimes contradictory. For instance in the case of AB Aur, the brightest and best-studied Herbig Ae/Be star, Mannings & Sargent infer an almost edge-on geometry, i = 76°, while Grady et al. claim i $\leq$ 45°. Furthermore, most of these imaging studies have been performed in the millimetre and radio regimes, probing the geometry on a relatively large scale,

between about 100 – 1000 AU. To make progress in the area of star formation for the higher mass stars, observations exploring the innermost regions around these objects are badly needed. Until sub-milli-arcsecond imaging becomes a reality, linear spectropolarimetry across emission lines such as Hα is the most powerful technique for doing so, as the scattering of starlight on electrons in an ionised medium occurs within a few stellar radii (Rudy 1978; Cassinelli, Nordsieck, & Murison, 1987).

This application of spectropolarimetry was first established in studies of classical Be stars (Clarke & McLean 1974; Poeckert 1975). In its simplest form, it is based on the expectation that Hα photons arise over a much larger volume than the stellar continuum photons. For this reason the line photons undergo fewer scatterings off e.g. a circumstellar disc than the continuum photons do. Consequently the emission line flux will be much less polarised than the continuum. In this situation, a change in polarisation across the line profile is expected – we refer to this *de*polarisation as the classical line effect (because of its first appearance in observations of classical Be stars). The high incidence of these line depolarisations among members of this object class (26 out of 44 in Poeckert & Marlborough 1976) indicated that the envelopes of classical Be stars are not spherically symmetric. These findings are now taken as compelling evidence that classical Be stars are embedded in circumstellar discs (see e.g. Waters & Marlborough 1992).

Since then, Hα spectropolarimetry has been performed on a variety of other strong line emitting objects, such as B[e] stars (Zickgraf & Schulte-Ladbeck 1989; Magalhães et al. 1992), Luminous Blue Variables (e.g. Schulte-Ladbeck et al. 1994), novae (Bjorkman et al. 1994) and supernovae (e.g. Cropper et al. 1988). In the case of pre-main sequence stars the technique has recently been applied to a sample of 9 Herbig Be stars by Oudmaijer & Drew (1999; hereafter OD99). The main outcome of this pilot study was that a line effect was detected in about half the Herbig Be stars. It is possible that the OD99 detection rate is consistent with discs around all these stars being viewed at angles ranging from face-on to edge-on. But to be able to make a proper distinction between viewing angle and intrinsic geometry effects, one needs to obtain a larger sample. We pursue this goal by increasing the sample of spectropolarimetric data to about 25 Herbig stars in total.

In addition to increasing the sample, we extend our data set toward the later spectral type Herbig Ae (HAe) stars, where we may be able to detect spectropolarimetry characteristics differing from the earlier type Herbig Be (HBe) stars. A switch in phenomenology may be expected to occur at some point working down the stellar mass range, as different physical mechanisms are likely to play a role at different spectral types. For instance, radiation pressure forces are likely to play a role for the higher luminosity stars at the early B types, whereas magnetic fields may become more dynamically prominent at the later A types. The magnetically-channelled accretion model (Ghosh & Lamb 1979) that is commonly applied to the lowest mass pre-main-sequence T Tauri stars (by e.g. Bouvier, Forestini, & Allain, 1997) may also be a suitable model as early as spectral type A (Pontefract et al. 2000). If it does operate, the inner accretion disc around the star is truncated by the magnetic field, and the depolarisation effect may then be absent because

the inner hole will necessarily lead to reduced intrinsic continuum polarisation. Alternatively, the channelled accretion may produce a relatively bright and compact source of Hα emission that may be scattered within the accretion column itself or within the disrupted disc. This in turn may yield a polarisation signature at Hα that is more complex than the simple depolarisation effect (see McLean 1979; Wood, Brown & Fox 1993). The second goal of this paper is accordingly to explore how the Hα spectropolarimetric signature behaves as a function of Herbig star spectral type.

The paper is organised as follows. In Sect. 2 we discuss the way in which our sample was selected, how the observations were performed, and reduced. In Sect. 3 we first present the continuum polarisation results for the whole sample and subsequently focus on the spectropolarimetry. We outline spectropolarimetric behaviour that can be expected, and develop tools to characterise the observations. We then discuss the individual targets, where we proceed by separating the discussion on the Herbig Be stars (Sect. 4.1) from the Herbig Ae stars (Sect. 4.2). The two groups are subsequently compared in Sect. 5. In Sect. 6 we summarise the main outcomes of our study and discuss the possible interpretations.

2   OBSERVATIONS

2.1   Sample selection

Our target stars were selected from the Herbig Ae/Be catalogue of Thé, de Winter & Perez (1994). Note that in the following only objects appearing in Table 1 from their catalogue will be discussed and considered in the statistics as "genuine" Herbig stars. Herbig (1960) originally selected these stars on the basis of three criteria, but more recently Waters & Waelkens (1998) stressed the importance of a dusty infrared excess. Most of the objects in Table 1 by Thé et al. follow the criteria, but a few objects may not have a dusty infrared excess. Yet, it is the largest representation of a genuine intermediate mass young population that is currently available.

All the targets from this list that we were then able to observe are listed in our Table 1, alongside their spectral types and V magnitudes, as listed in SIMBAD. It is important to note that the targets were not selected with any foreknowledge of flattened circumstellar geometries, but were selected because of their relative brightness ($V \lesssim 11$) and their position on the sky.

2.2   Spectropolarimetric observations

The linear spectropolarimetric data were obtained during the nights of 1999 December 18 – 20 using the ISIS spectrograph mounted on the Cassegrain focus of the 4.2-metre William Herschel Telescope (WHT), La Palma. For all observations a slit width of 1.2″ was used. Although the sky was relatively clear, the seeing was rather poor ($\sim 1.5 - 3''$). We used a 1024 × 1024 pixel TEK-CCD detector with the 1200R grating, which yielded a spectral coverage from 6370 – 6760 Å. This coverage corresponds to a spectral resolution of approximately 35 km s^{-1} around Hα (as measured from arc line fits).

To be able to analyse the linearly polarised component

Table 1. Herbig Ae/Be targets. *V* magnitudes (column 3) and Spectral types (column 4) are taken from SIMBAD. The integration times denote the total exposures (column 6). The errors in our polarisation data (column 7) are of the order of 0.01% based on photon-statistics only. Yet, systematic (external) errors in the polarisation are estimated to be 0.1%. The errors in the Position Angle θ (column 8) are less than a degree. Column (9) gives estimates of the sky PA derived from line excursions; note that the presumed discs are supposed to lie perpendicular (=90°) to this determined sky PA.

Name	HD Number	V	Spec. Tp	Date	Exposure(s)	$P_{\mathrm{cont}}^{\mathrm{R}}$ (%)	$\Theta_{\mathrm{cont}}^{\mathrm{R}}$ (°)	$\Theta_{\mathrm{intr}}^{\mathrm{R}}$ (°)
MWC 137		11.2	Be	20-12-99	24x100	6.07	160	115 ± 10
MWC 1080		11.6	B0	18-12-99	8x500	1.73	77	
MWC 166	HD 53367	7.0	B0	18-12-99	16x150	0.20	34	
BD+40 4124		10.7	B2	19-12-99	24x100	1.21	8	173 ± 8
MWC 361	HD 200775	7.4	B2Ve	18-12-99	16x100	0.81	96	
IL Cep	HD 216629	9.3	B2IV-Vne	19-12-99	16x100	4.24	102	
MWC 147	HD 259431	8.8	B6pe	18-12-99	24x50	1.05	100	
MWC 158[1]	HD 50138	6.6	B9	18-12-99	16x20	0.65	59	45 ± 5
	HD 58647	6.8	B9IV	19-12-99	16x75	0.14	127	
AS 477		10.2	B9.5Ve	19-12-99	16x150	0.43	56	
MWC 120	HD 37806	7.9	A0	19-12-99	16x50	0.35	76	
KMS 27	HD 37357	8.9	A0	19-12-99	16x200	0.13	52	
MWC 789	HD 250550	9.6	A0	20-12-99	32x100	0.92	174	178 ± 10
AB Aur	HD 31293	7.1	A0pe	18-12-99	16x150	0.11	54	160 ± 5
SV Cep		10.1	A0	20-12-99	8x500	0.61	67	
XY Per	HD 275877	9.4	A2II	20-12-99	8x300	1.60	132	
MWC 480	HD 31648	7.7	A2	19-12-99	16x75	0.38	52	
	HD 244604	9.4	A3	19-12-99	16x200	0.44	119	
MWC 758	HD 36112	8.3	A3	19-12-99	16x100	0.07	179	
T Ori		9.5	A3V	20-12-99	8x500	0.39	97	
	HD 245185	10.0	A5	20-12-99	8x500	0.21	168	
	HD 35929	8.1	A5	19-12-99	16x200	0.12	51	
CQ Tau[2]	HD 36910	10.7	F2IVe	20-12-99	8x500	0.27	83	

[1] MWC 158 does not appear in Table 1 of Thé et al. (1994). The data have been included for completeness.
[2] Note that the spectral type for CQ Tau as given by Thé et al. (1994) is between late A and early F (A8 – F2), and
   is indeed considered to be a member of the Herbig Ae/Be group.

in the spectra, ISIS was equipped with the appropriate polarisation optics. This consisted of a rotating half-wave plate and a calcite block to rotate and separate the light into two perpendicularly polarised light waves – respectively the ordinary (O) and extraordinary (E) rays. Two holes in the Dekker also allow for simultaneous observations of the object and the sky. Hence, for each exposure, four spectra are recorded: the O and E rays of both the target and sky. One complete observation set consists of a series of four exposures at half-wave plate position angles of, in chronological order, 0°, 45°, 22.5°, and 67.5° to obtain the linear Stokes parameters Q and U. After each of these sets of four frames were obtained, the holes in the Dekker for the target and the sky were interchanged to compensate for any kind of asymmetry in either the detector or the instrument. To prevent the CCD from saturating on the peak of Hα, shorter exposure times were adopted for those objects with strong Hα emission. Finally, polarised and zero-polarisation standards were observed regularly, revealing an intrinsic instrumental polarisation of the order of 0.1 per cent, which we do not correct for, as our aim is only to investigate Hα polarimetric signatures relative to the continuum.

2.3 Data reduction and calibrations

The reduction of the data was carried out using IRAF (Tody 1993). The data reductions steps included the usual (i) bias-subtraction, (ii) flat-fielding, (iii) cosmic ray removal, (iv) extraction of the spectra and (v) wavelength calibrations of the O and E spectra.

The E and O ray data were then imported into the polarimetry package CCD2POL, incorporated in the FIGARO software package maintained by STARLINK. The Stokes parameters Q and U were determined, leading to the percentage linear polarisation P and its Position Angle (PA) θ in the following way:

$$P = \sqrt{(Q^2 + U^2)} \qquad (1)$$

$$\theta = \frac{1}{2} \arctan\left(\frac{U}{Q}\right) \qquad (2)$$

Note that a PA of 0°, i.e. North-South, on the sky is represented by a vector that lies parallel to the positive Q axis, whereas $\theta = 90°$ (i.e. East-West) is positioned in the negative Q direction. Positive and negative U axes thus correspond to position angles of respectively 45° and 135°.

The data were subsequently analysed using POLMAP. This package was also used to remove an instrumental, wavelength-dependent ripple (see Harries & Howarth 1996 for a discussion on the derippling procedure). The success of this last step in the data extraction is occasionally less than complete, such that we will have to comment on a few instances where some ripple seems to have remained. The achieved (relative) accuracy of the polarisation data is in principle only limited by photon-statistics and can be very small (typically 0.01 %). However, the quality and the

amount of data taken on spectropolarimetric standard stars is at present not yet sufficient to reach absolute accuracies below 0.1% (see the manual by Tinbergen & Rutten, 1997). In most parts of the paper the spectropolarimetric data are shown binned to a constant error of 0.05% polarisation and therefore the presented polarisation spectra exhibit a spectral resolution that depends on the total number of counts (i.e. along the Hα profile, the highest resolution is achieved at the wavelength of the emission peak). In a few cases, we choose to slightly modify the error per bin in order to achieve the best compromise between minimising the error per bin and resolving the line profiles.

Just as we do not correct for instrumental polarisation, no correction for interstellar polarisation (ISP) is made either. This is because the ISP only adds a wavelength-independent polarisation vector to all observed points when plotted in (Q, U) space. Precisely because of this wavelength independence, we will particularly rely on the (Q, U) plane representation of the data in classifying the type of Hα polarisation signature.

3   GENERAL RESULTS

We begin with a brief presentation of the continuum polarisation results (Sect. 3.1), before we focus on the spectropolarimetry (Sect. 3.2). The discussion of individual targets is performed in the next section (Sect. 4).

3.1   Continuum Polarimetry

The linear polarisation of Herbig Ae/Be star continua can be attributed to the scattering of stellar photons off matter within an asymmetric circumstellar geometry. In addition there may be a substantial interstellar contribution. It is not yet settled which polarigenic agent causes the circumstellar polarisation, but the most likely candidates are dust particles and electrons. Whilst the resolution of this question is both interesting and significant, we leave it for the future, given our present focus on the implications of the line polarisation morphology for the circumstellar geometry.

The measured continuum polarisations for both the HBes and HAes are summarised in Table 1. The mean percentage polarisation and position angle obtained for each object appear in columns (7) and (8). In addition, for cases where an excursion in (Q, U) space (see later) is present, we estimate the sky PA from these line excursions, and present them in column (9) for completeness. (Note that the presumed discs are supposed to lie perpendicular to these sky PA estimates).

Polarisation variability is a well-known and common phenomenon (Vrba, Schmidt & Hintzen, 1979; Grinin 1994). In general terms, it is viewed as caused by time variable amounts and/or projected distributions of circumstellar gas and dust. Accordingly we do not look for perfect agreement between our continuum polarisation measurements and those in earlier literature. Nevertheless, the values of the polarisation quantities, %Pol and PA, are generally consistent with previous continuum measurements in the R band (Petrova & Shevchenko 1987; Jain & Bhatt 1995; OD99; and Oudmaijer et al. 2001).

3.2   Spectropolarimetry

The observed Hα characteristics of each Herbig star are listed in Table 2. The first few columns list the Hα parameters deducible from the "intensity" (Stokes I) profile only, namely the equivalent width (EW; column 2) and the ratio of the peak line counts over the continuum counts (column 3). These parameters can be used as indicators for the amount of ionised gas in the environments of these objects. As one would expect, these quantities show a general decline toward later spectral types.

The spectroscopic line shapes of the Herbig stars vary from pure emission, double-peaked emission, P Cygni type, through to inverse P Cygni type. We will see later that these spectroscopic line profiles do not necessarily correlate with the spectropolarimetry. In fact, spectropolarimetric behaviour seems to be rather more homogeneous than Stokes I spectroscopy. This is illustrative of how the polarised light contribution to the total light has a more selective scattering origin. It is an independent dimension of information on the source geometry. In other words, spectropolarimetric line profiles offer the opportunity to study physical phenomena that are unobservable in normal spectroscopy.

Columns (4) to (8) in the Table concern spectropolarimetric properties. Plots of the spectropolarimetric data for the Herbig Ae/Be stars are presented in the different panels of Figs. 4 and 5. For all objects the polarisation spectra are presented as triplots (consisting of Stokes I, P, and θ), as well as loci in (Q, U) space.

3.2.1   Spectropolarimetric expectations

Consider a star embedded in an at least partly ionised circumstellar medium. If (part of) the Hα photons are formed over a large volume, and the projected distribution of Thomson-scattering free electrons is sufficiently flattened on the sky, the line emission itself is unpolarised while the continuum shows some linear polarisation. One may then expect to detect a depolarisation line effect (as found in classical Be stars). Where this happens one would expect to see a change in %Pol across the line that more or less "follows" the shape of the Stokes I intensity profile. Hence the polarisation change is expected to be as broad as the line emission itself (see the middle panel of the triplot sketch in Fig. 1). In this case the depolarisation across Hα is only seen in the %Pol, but in practise (due to the vector addition of the foreground polarisation), it may be observable in the PA as well or instead. In any case, when mapped onto (Q, U) space, the line wavelength points will emerge from the continuum knot as a linear excursion (as seen in the (Q, U) plane sketch of Fig. 1).

If, on the other hand, (part of) the Hα line photons originate from a *compact* rather than an extended source, one may pick out more subtle line effects, as have for instance been modelled by Wood et al. (1993; see also McLean 1979). In the presence of a compact Hα source one can envision a variety of line effects that will map into (Q, U) space in as many ways. The patterns seen will depend on the specific geometry and bulk motions of the scattering particles surrounding the compact Hα source. If the scattering occurs predominantly in a rotating disc-like configuration, the subsequent breaking of left-right reflection symmetry in the ve-

Table 2. The Hα line results. The errors on the equivalent widths of the Hα lines (column 2) are below 5%, the errors on $\Delta\lambda$(Pol) (column 5) and $\Delta\lambda(I)$ are determined at Full Width Zero Intensity (FWZI) and are about 10%. $\Delta\lambda$(Pol) has been defined as the width over which the polarisation changes. In the case where the widths in PA and %Pol are unequal, we take the largest of the two. The fractional width ($\frac{\Delta\lambda(\text{Pol})}{\Delta\lambda(I)}$) is given in Column (6). The followed recipe with regard to the depolarisation question (column 7) is described in the text. Column (8) represents the morphology in (Q,U) space.

Object	Hα EW(Å)	Line/Cont Contrast	Line Effect?	$\Delta\lambda$(Pol) (Å)	($\frac{\Delta\lambda(\text{Pol})}{\Delta\lambda(I)}$)	Depolarisation?	(Q,U) behaviour	Spectral Type
MWC 137	−404	70	yes	55	0.92	yes	exc	B
MWC 1080	−101	18	yes	50	1.11	yes	smear	B0
MWC 166	−2.8	1.6	no?	–	–	–	–	B0
BD+40 4124	−113	17	yes	30	0.75	yes	exc	B2
MWC 361	−63	8.5	yes	45	1.13	yes(+)	exc	B2
IL Cep	−20	3.5	no	–	–	–	–	B2
MWC 147	−60	13	yes	18	0.50	no	exc	B6
HD 58647	−8.6	2.4	yes	10	0.67	no	loop	B9
MWC 120	−29	6.3	yes	13	0.65	no	loop	A0
MWC 789	−46	10	yes	21	0.95	no	loop+exc	A0
AB Aur[1]	−40	8.0	yes	17	1.00	no	loop+exc	A0
XY Per	−6.7	2.3	yes	15	0.88	no	loop	A2
MWC 480	−21	4.8	yes	12	0.67	no	loop	A2
HD 244604	−14	4.5	yes	10	0.56	no	loop?	A3
MWC 758	−17	4.0	no	–	–	–	–	A3
T Ori	−12	3.9	yes	5	0.26	no	loop	A3
HD 245185	−17	3.7	yes	10	0.56	no	loop	A5
HD 35929	−3.2	2.0	no	–	–	–	–	A5
CQ Tau	−2.7	1.6	yes	3	0.17	no	loop	F2
MWC 158	−54	12	yes	25	1.0	no	exc	B9
AS 477[2]	−19	4.4	no?	–	–	–	–	B9.5
KMS 27[3]	−7.2	2.5	yes	–	–	–	–	A0
SV Cep[2]	−13	2.5	yes	–	–	–	–	A0

[1] For AB Aur an improved data reduction sequence was followed in comparison to the data presented in Pontefract et al. (2000); the conclusions reached in Pontefract et al. remain valid.

[2] The data on AS 477 and SV Cep suffer from too low photon counts to interpret them.

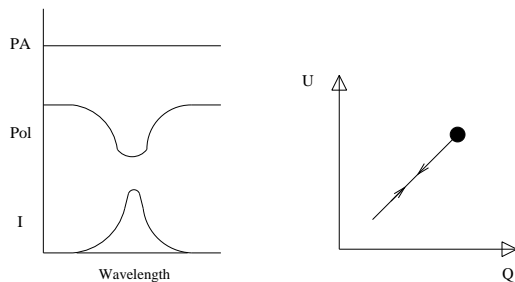[3] The smear in KMS 27 is due to the broad photospheric absorption wings.

Figure 1. Cartoon: depolarisation across Hα; seen in a triplot and a (Q,U) diagram. A typical Stokes I emission is shown in the lower panel of the triplot, the %Pol in the middle panel, while the Position Angle is sketched in the upper panel of the triplot. Note that the depolarisation across Hα is as broad as the Stokes I emission. Depolarisation translates into (Q,U) space as a linear excursion.
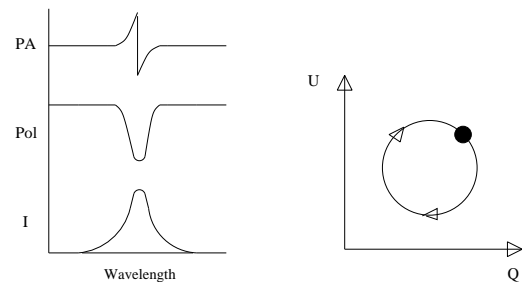

Figure 2. Cartoon: compact Hα scattered in rotating disc. Note that the polarisation signatures are relatively narrow compared to the Stokes I emission. The flip in PA is associated with a loop in (Q,U) space.

locity field leads to a changing PA with wavelength (McLean 1979), which appears as a "loop" in (Q,U) space (see the cartoon in Fig. 2). If the scattering however occurs in an expanding (as opposed to a rotating) medium, there is no

breaking of the left-right symmetry, and the track in (Q,U) space will appear to be more "linear". In case of a rotating *and* an expanding medium, the tracks in (Q,U) space are expected to appear as a combination of the two and thus be more or less "hook-shaped" (see Schulte-Ladbeck et al. 1994; Oudmaijer et al. 1998). In all of these compact Hα cases there is the possibility that the width of the polarisa-
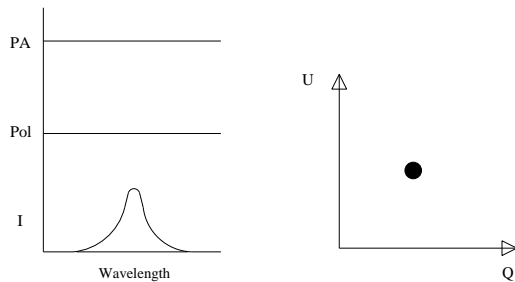
Figure 3. Cartoon: "no line effect"

tion profile across Hα does not coincide with the width of the Stokes I intensity profile (see the triplot sketch in Fig. 2).

Finally, where the geometry on the sky is circular, as is the case for either spherically symmetric geometry or a face-on disc, there is no change in PA and/or %Pol across the line. In this circumstance and in the ideal limits of noiseless data and no wavelength dependence of foreground polarisation, all points in (Q, U) space would collapse into a single "dot" (see Fig. 3). For some objects described below there is no Hα line effect apparent in the triplot, but yet due to polarisation changes in the continuum or broad photospheric absorption wings the "dot" smears to a short fuzzy line, called a "smear".

3.2.2 Spectropolarimetric Tools

Inspecting the different objects in Figs. 4 and 5 one finds a range of morphology in the polarisation spectra (triplots), as well as in the (Q, U) plots. Most importantly, 15 out of the 22 Herbig stars show a clear variation across the Hα line. (The only objects that do definitely not show any changes across Hα at all in our data are IL Cep, MWC 758, and HD 35929). The question whether or not a line effect is present or not is answered qualitatively in column (4) of Table 2. The high number of line effect detections is interesting in its own right, given that any polarisation change across a line indicates scattering off a geometry, that, in projection on the sky, deviates from spherical symmetry.

Although the morphology in both the polarisation triplots and (Q, U) space shows some variety, we will classify them according to their common characteristics. To this end, we have developed several tools to characterise the line effects. One such tool involves the fractional line width over which the polarisation changes (see data in columns 5 and 6 in Table 2). In cases where the widths of the PA and %Pol changes are unequal, we choose the largest in specifying the change $\Delta\lambda(\text{Pol})$ (column 5). This then is divided by the width of Stokes I, $\Delta\lambda(I)$ to yield a dimensionless measure of polarisation width (column 6). Note that both $\Delta\lambda(\text{Pol})$ and $\Delta\lambda(I)$ are measured at full width–zero intensity (FWZI).

The other, more qualitative, tool concerns the *shape* of the polarisation change across the line (columns 7 and 8). Whether or not the change in polarisation across Hα is consistent with the depolarisation mechanism is noted in column (7). To limit our subjectivity, we have constructed a recipe for answering this question that proceeds as follows. First, the line effect needs to be broad enough to be consistent with a depolarisation. If the ratio ($\frac{\Delta\lambda(\text{Pol})}{\Delta\lambda(I)}$) is smaller

than a value of 0.75 we claim that the line effect is not consistent with the depolarisation mechanism, and the answer in column (7) is simply a "no". If however, the ratio ($\frac{\Delta\lambda(\text{Pol})}{\Delta\lambda(I)}$) has a value larger than 0.75, the polarisation change could indeed be due to depolarisation, but not necessarily. We therefore employ a second criterion that takes into account the finer details of the line effects. In many cases a so-called "flip" in PA and/or %Pol across the line will be clearly noticeable. In case this occurs the line effect can not be due to depolarisation and the answer in column (7) should also be "no". If, on the other hand the behaviour in %Pol and/or PA is monotonic, and ($\frac{\Delta\lambda(\text{Pol})}{\Delta\lambda(I)}$) is larger than 0.75, the answer to the question "Is the line effect due to depolarisation?" can be answered convincingly with a "yes".

As the shapes of the line polarisations are so nicely represented as loci in (Q, U) space, we also classify the (Q, U) plane morphologies. These are given in column (8) of Table 2. In every case we expect there to be a dark knot of points that arises from the sampling of the continuum polarisation. Where the morphology also includes a rounded loop the term "loop" appears in column (8) of Table 2. The word "dot" is given when no line effect is present, and finally in case there is a more or less linear excursion arising from the continuum knot, we refer to this excursion with "exc". For convenience, the spectral types of the objects are listed in column (9).

4 INDIVIDUAL TARGETS

First, we add to OD99's sample of Herbig Be stars (Sect. 4.1), and then we turn attention to the later-type, and presumably less-massive Herbig Ae stars (Sect. 4.2). A comparison between the spectropolarimetric signatures of HAe and HBe stars is made in Sect. 5.

4.1 The Herbig Be stars

The Hα line profile data obtained for the Herbig Be stars are presented in Fig. 4. Six out of eight HBe stars in Fig. 4 show a clear line effect, whereas only two cases (IL Cep and MWC 166) do not show a line effect at all. Note that two stars (MWC 158 and AS 477) are not included in this statistics, for reasons discussed later on. The size of this sample can be increased by including the data on the HBes from OD99. The sample of Herbig Be stars in OD99 consists of nine HBe stars, of which four stars are in common with the present study, which would leave us with five HBes to be added to the eight in the current study. However the number of photons counts for Lk Hα 218 is regarded as insufficient and the object is thus dropped, leaving us with a total of (8+4) 12 HBes. As these four added HBes from OD99, namely V380 Ori, ω Ori, GU Cma and MWC 297 are all cases of no discernible polarisation changes across the line, we would find that 6 out of 12 Herbig B stars show a line effect. But, as the OD99 and the current data were obtained at different epochs, spectropolarimetric changes may be seen in the targets common to both studies. We omit a discussion of such variability in this paper, but note that most of the objects in OD99 classified as having a line effect exhibit one here as well. Yet, there is an exception. In the case of MWC 166 (HD 53367) the line effect noted by OD99
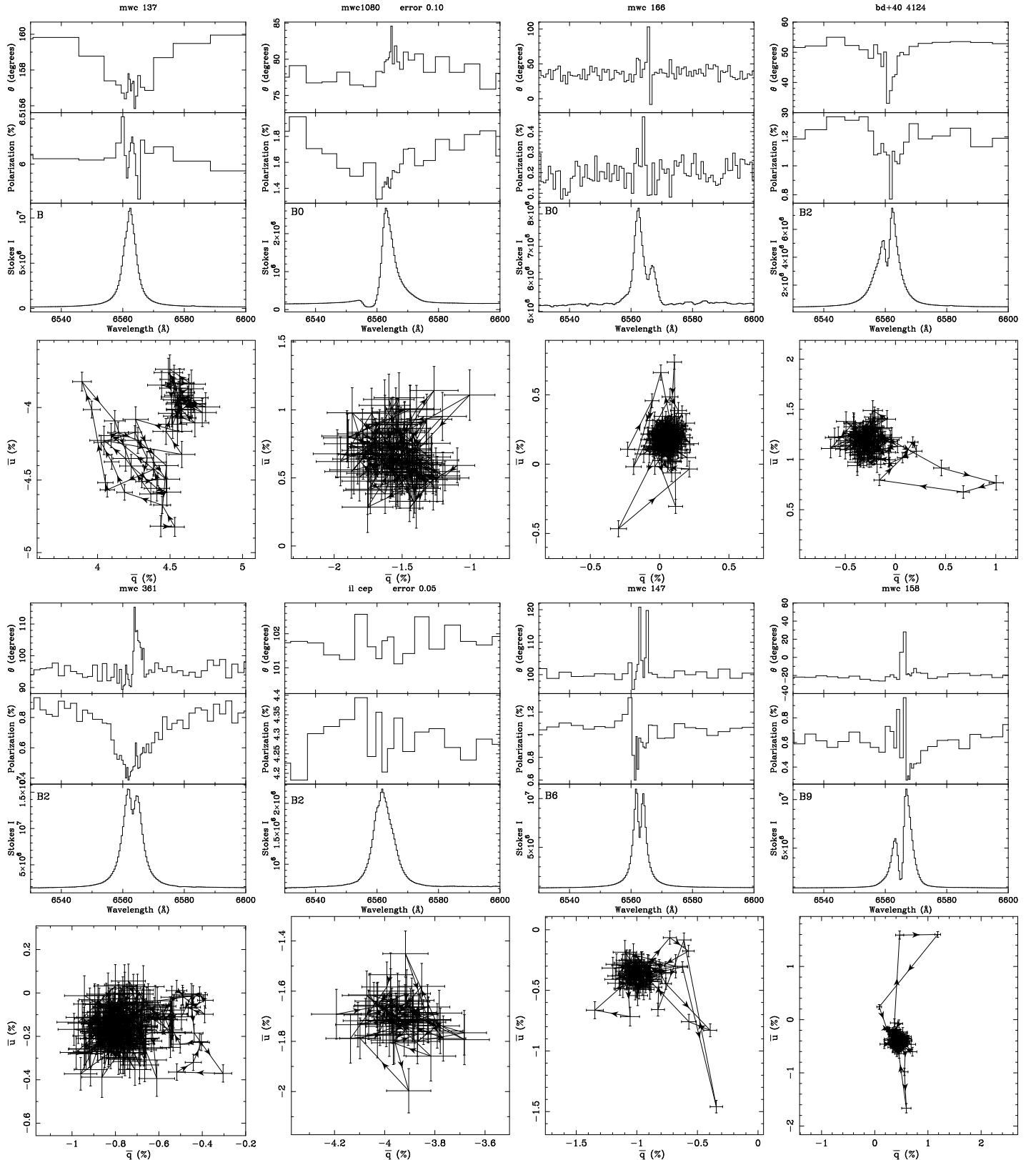
Figure 4. Polarisation spectra of Herbig Be stars and their (Q, U) diagrams (below the triplots). For each star the Stokes I spectrum is shown in the lowest panel of the triplot, the %Pol in the middle panel, while the PA (θ; see Eq. 2) is plotted in the upper panel. The data are rebinned such that the 1σ error in the polarisation corresponds to 0.05% as calculated from photon statistics. In case of exceptions on this, the polarisation errors are given on top of the triplots. The spectral types are indicated in the Stokes I plots for convenience. The lower plot represents the normalised Stokes parameters $u = U/I$ against $q = Q/I$. Note that the binning errors in these (Q, U) plots are consequently multiplied by a factor of two (compared to the binning errors in the triplots) to present a well-defined continuum.

Figure 4. Continued

has disappeared. Although there is the possibility that what was once a detectably flattened circumstellar geometry has become more circular in projection onto the sky, it is more likely that the change is due to a reduced amount of ionised particles. Given that the new data show a large fall in the Hα equivalent width (now −2.8Å rather than −14Å as in OD99), it is likely that the reduced ionisation level resulted in fewer electron scatterings. Adding MWC 166 as a line effect case, we finally find that 7 out of 12 HBe stars show a line effect. This incidence of line effects among the HBe objects may be compatible with a picture in which all HBes are embedded in flattened geometries on small scales. The explanation for the non-detections is then simply the consequence of an expected number of close to face-on-viewing angles, liable to produce too weak a polarisation to be detected.

Let us briefly discuss the polarisation spectra (and (Q, U) diagrams) of all the Herbig Be stars, as displayed in the different panels in Fig. 4.

Objects showing a depolarisation: *MWC 137, MWC 1080, BD+40 4124 and MWC 361.* These are all objects where at Hα at least one of the two polarisation signatures – as presented by %Pol and/or PA – follows the shape of the Stokes I line profile monotonically. The width over which the polarisation change occurs is also relatively broad, resulting in a ratio $(\frac{\Delta\lambda(\mathrm{Pol})}{\Delta\lambda(I)})$ larger than 0.75. Therefore these objects may indeed be interpreted as undergoing a line depolarisation associated with continuum polarisation caused by scattering off an ionised disc on small spatial scales. In the case of MWC 137, with its exceptionally high line/continuum contrast, the ripple correction (derived from

the continuum) may not have been good enough to remove all ripple from the polarisation spectrum, as seems to be the case near line centre in both the %Pol and PA spectra. This deficiency is responsible for the chaotic appearance of the (Q, U) plane excursion. Yet, as the shape of the PA clearly follows the Stokes I line, the object can surely be regarded as being subject to depolarisation. The %Pol in the spectrum of MWC 1080 follows the shape of the Stokes I line profile, and the object can thus also be considered as an example of depolarisation. For this object the (Q, U) diagram does not yield much additional information because of the smear of points due to the changing continuum polarisation. For BD+40 4124 both the PA and the %Pol follow the intensity profile, consistent with the depolarisation picture. Although the %Pol of MWC 361 shows a classical depolarisation across the line, the change in PA is rather less straightforward. Specifically, the blue wing does not show any sign of a change in PA, while the innermost red wing shows a flip and then a return to the local continuum PA in the far wing. We come back to this unusual case in the discussion in Sect. 6.

Objects showing a complex line effect: *MWC 147 and HD 58647.* The late B type objects MWC 147 and HD 58647 both show polarisation changes wherein $(\frac{\Delta\lambda(\mathrm{Pol})}{\Delta\lambda(I)})$ is significantly smaller than 1. Also, in the (Q, U) plane the polarisation changes across the line do not present as simple linear excursions.

Objects showing no clear line effect: *IL Cep, MWC 166, AS 477.* In a few cases we must classify the B star as not showing a line effect. In the case of
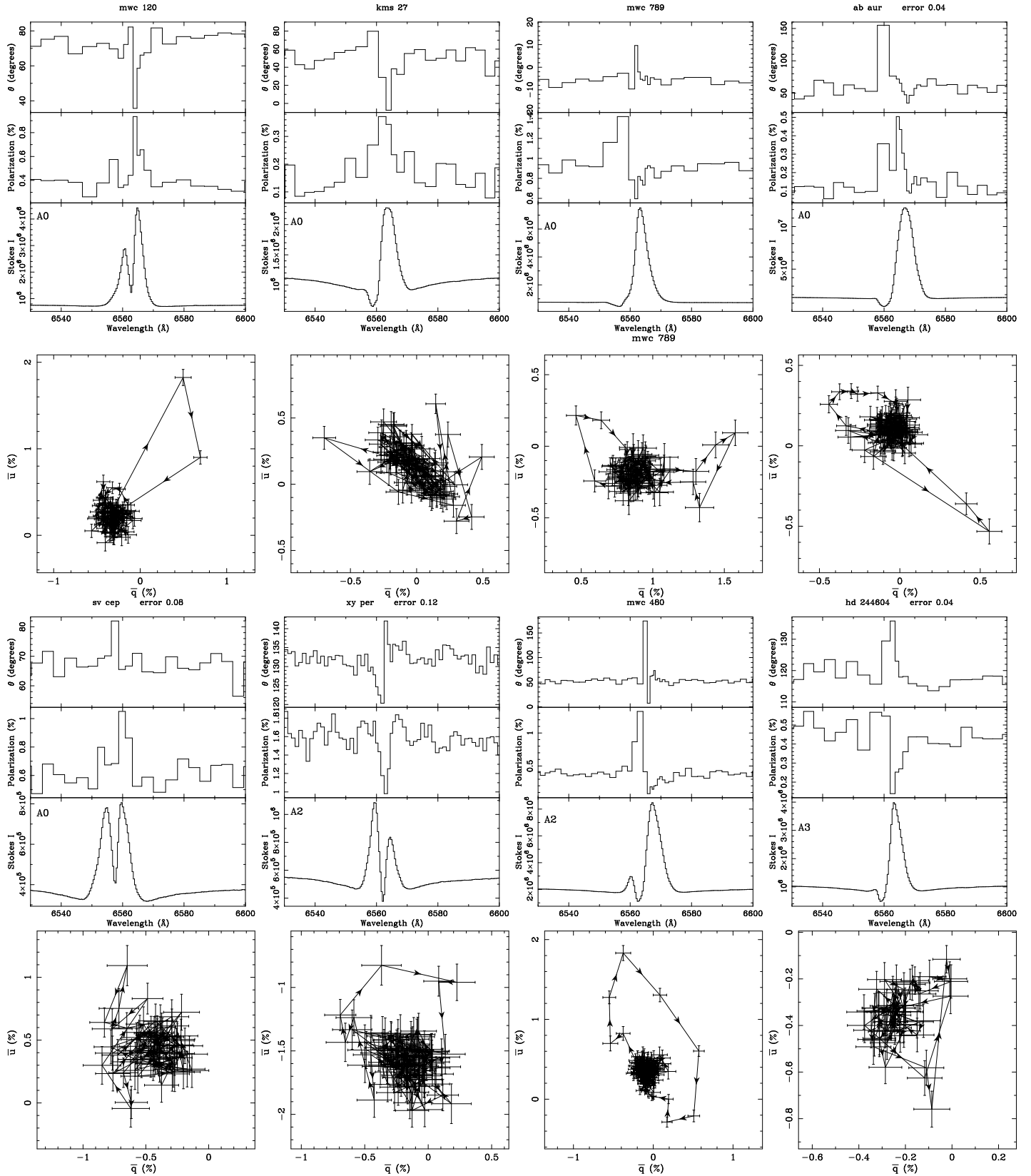
Figure 5. Polarisation spectra of Herbig Ae stars and their (Q, U) diagrams. See the caption of Fig. 4 for further details.
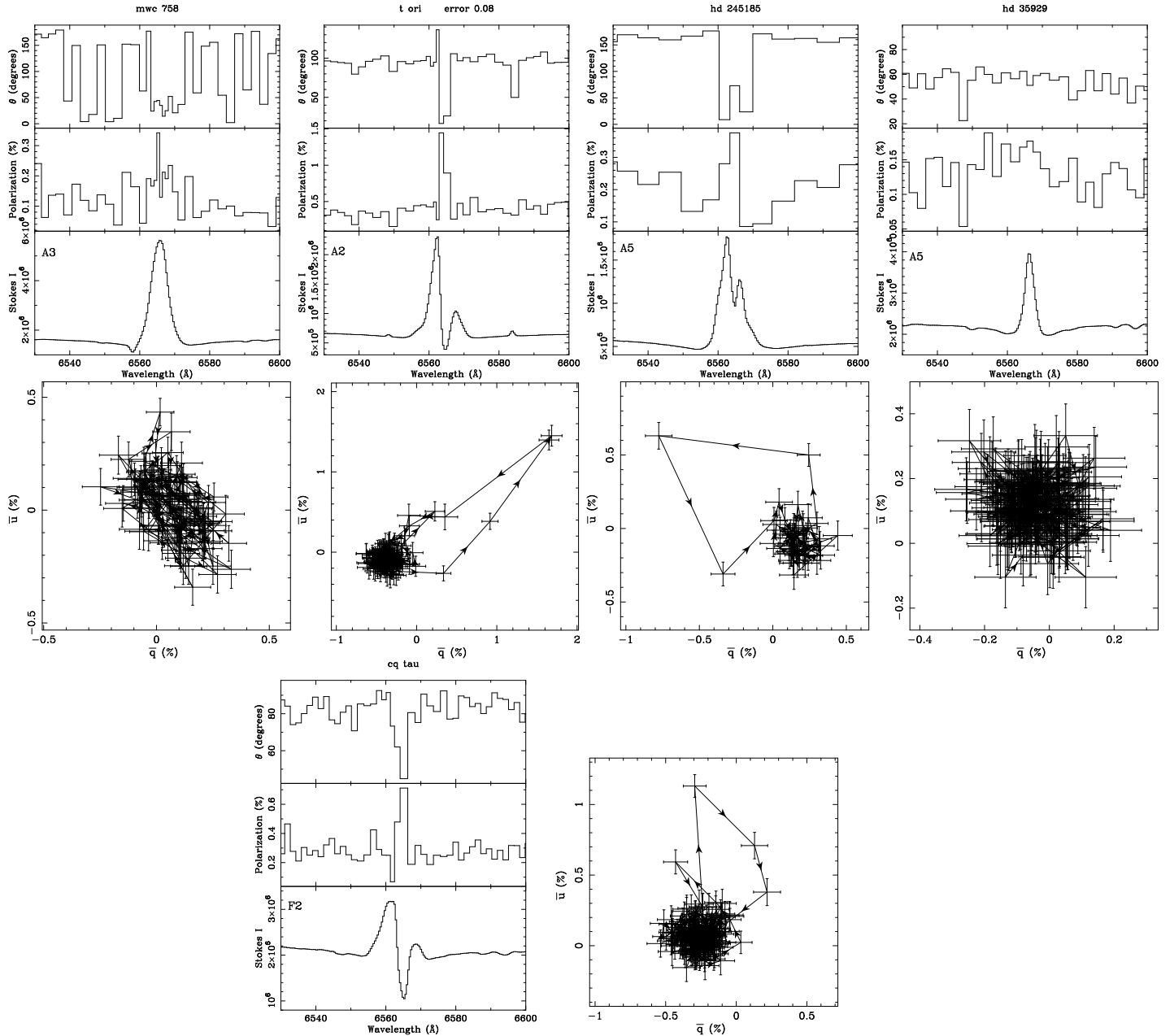
Figure 5. Continued

IL Cep this is unambiguous, but due to the low signal for AS 477 the data are not convincing one way or the other. Therefore we do not regard this object in our statistics and place a question mark in column (4) against this star in Table 2. Note that for MWC 166 one may possibly believe that there is a residual polarisation change across the line, but we view the change as too narrow to be credible.

4.2 The Herbig Ae group

The spectropolarimetric data for the HAes are presented in Fig. 5. The first thing that is striking is the – perhaps unexpected – high number of line effects, namely in 9 out of the 11 targets for which the data quality allows sufficient

definition. This is even higher than for the HBe sample. Furthermore, there seems to be a difference in the character of the polarisation changes compared to those seen in the HBe stars. As for the HBe stars, we now present our classification of these results.

Objects showing a loop: *MWC 120, XY Per, MWC 480, T Ori, HD 245185, and CQ Tau.* There are certainly 4 instances of very well formed loops in the (Q, U) plane. In the triplots these correspond to the line-centre flips (and neighbouring points) in either %Pol or PA. MWC 480, a relatively bright HAe star, is a particularly fine example. Although the loops associated with T Ori and MWC 120 are sufficiently elongated that they might alternatively be described as more akin to excursions, the complexity of the changes apparent in the triplots strengthens the

similarity with the clear-cut examples of "loops" – hence their inclusion here.

Objects showing a loop and excursion: *MWC 789 and AB Aur.* Two stars in the HAe groups show a behaviour in (Q, U) space that is more complex than the presence of just a loop. These cases are MWC 789 and AB Aur. Both are objects where the Hα line profile includes a blueshifted absorption component: it is this part of the line profile that maps onto the (Q, U) plane as a more linear excursion. The rounded loop in both is then associated with the redshifted line emission. A fuller discussion of this morphology is given in Pontefract et al. (2000).

Objects showing no line effect: *MWC 758 and HD 39529.* In these two cases the data are good enough that we can claim no evidence of any kind of line effect.

Objects in need of better observations: *KMS 27 and SV Cep.* For these two objects the quality of the data is relatively poor and hence their interpretation is more difficult. The data on SV Cep suffer from a too low signal, just as was the case for AS 477 in the HBe group. KMS 27 suffers from a "smear" in (Q, U) space, which is due to the broad photospheric absorption wings. In view of the above, the objects KMS 27 and SV Cep are dropped from our statistical overview.

5 TRENDS AND DIFFERENCES AMONG THE HERBIG AE/BE STARS

The motivation behind this observational study is to discover if there is any dependence of the geometry of the near-stellar environment of Herbig Ae/Be stars upon spectral type.

First we restate the raw statistics of the frequency of detectable linear polarisation changes across Hα among the Herbig Be stars, as compared with the Herbig Aes. We found that about half of the HBe stars had detectable changes across the line (7 out of 12 to be precise), while this "success rate" rises to a more impressive 9 out of 11 among the HAe stars. Note that the present sample sizes are not yet large enough for this difference to be formally significant.

A second attribute that shows some dependence on spectral type is the fractional width of the Hα line profile over which the polarimetric change occurs, specifically the quantity $(\frac{\Delta\lambda(\text{Pol})}{\Delta\lambda(I)})$. These fractional widths – as listed in column (6) of Table 2 – tend to decrease toward later spectral type. To visualise this, we have plotted the fractional widths in Fig. 6. There is much scatter, in part due to the difficulty of measurement, but presumably also due to real physical scatter. Nevertheless, it is apparent that the fractional widths for e.g. the B0-B2 HBe stars tend to be higher than those observed at spectral types later than A0: the means for these two sub-groups are respectively $(\frac{\Delta\lambda(\text{Pol})}{\Delta\lambda(I)}) = 1.0 \pm 0.2$ and 0.5 ± 0.3.

Of greater significance is that the Herbig Ae and Be stars present distinct kinds of Hα signature. This can be seen by comparing Figures 1 and 2 and also by scanning the morphology descriptors in columns (7) and (8) of Ta-
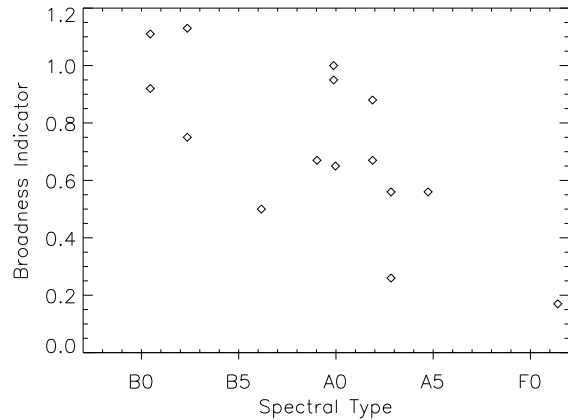

Figure 6. The fractional width ($\frac{\Delta\lambda(\text{Pol})}{\Delta\lambda(I)}$) plotted against spectral type. The errors on the broadness indicator ($\frac{\Delta\lambda(\text{Pol})}{\Delta\lambda(I)}$) are about 10 per cent.

ble 2. We note that, among the earlier Herbig Be stars, the phenomenon we have labelled depolarisation is the norm for stars presenting a clear line effect. We remind this is the behaviour that is also seen in classical Be stars. In contrast to this, there is a marked predominance of more rounded "loops" in the (Q, U) plane plots for the HAe stars (seen in only one HBe star, the B9 object HD 58647). In %Pol and PA as functions of wavelength, these loops correspond to antisymmetric flips. It was argued earlier that such behaviour may point to intrinsic Hα line polarisation that, in turn, most likely demands a compact source of Hα emission in these objects. The fact that $(\frac{\Delta\lambda(\text{Pol})}{\Delta\lambda(I)})$ tends to be noticeably less than one for these objects (Fig. 6) is consistent with this idea since the interior polarised line emission could well be narrower than the brighter exterior unpolarised component.

Among the HAe stars, and where the intensity profile includes a P Cygni blueshifted absorption component, the above-mentioned loops can be accompanied by a second (Q, U)-plane excursion on the opposite side of the continuum knot (i.e. at a relative angle of 90° in the plane of the sky). Examples of this are AB Aur and MWC 789. In both cases, the "loop" is due to the polarisation change across the central/redshifted line emission, while the second orthogonal "excursion" is associated with the blueshifted absorption. Similar excursions may be present on their own in T Ori and CQ Tau where the polarisation change is associated with significant redshifted absorption.

From the above we find two limiting patterns of behaviour: (i) in the early B group (B0 – B2) broad polarisation changes are observed across Hα that are consistent with depolarisation; (ii) in the later A stars (A2 – F), the line effects associated with Hα emission tend to be narrower than the Stokes I profile, and loops are seen in the (Q, U) plane. In between these two extremes we find transitional objects for which we have too few examples to be able to derive a general impression. It has to be regretted that later B spectral types remain poorly sampled as it would be interesting to see how the transition from early B-type to the A-type Hα polarisation characteristics is accomplished. Whether the detected difference between the HBe and the HAe stars is due

to different physics in the HRD or instead due to some observational bias effect is now open for discussion.

6 SUMMARY & DISCUSSION

Altogether we have found that 16 out of 23 Herbig Ae/Be stars show a change in linear polarisation across Hα. Data on 19 objects have been presented here, and are supplemented by 4 more from OD99. Summarised:

- For the Herbig Be stars: 7 out of 12 reveal a line effect that is consistent with a depolarisation effect caused by a flattened structure in analogy to the presence of discs around classical Be stars.
- For the Herbig Ae stars: 9 out of 11 show a line polarisation effect characterised by a "loop" in (Q, U) space, which suggests compact Hα emission that is itself polarised by a rotating disc-like medium.

We have found that the changes detected in the Herbig Be stars are like those observed in classical Be stars. It is worth considering whether this 7/12 (or ∼58 percent) detection rate is also as high as found among classical Be stars. Before making such a comparison, it is necessary to establish the typical sensitivity limit of our spectropolarimetry. This is most easily derived by assessing the radii of the continuum knots in the (Q, U) plane plots: typically these are large enough that excursions out of them that extend no further than 0.2% are too unclear to claim as definite detections. Using this as the detection threshold for polarisation changes across Hα, we can turn for a comparison to the large classical Be sample of Poeckert & Marlborough (1976). They tabulated the change in line polarisation percentage across Hα for 48 classical Be stars (their Table 2). In 26 of these stars, the polarisation change was greater than our sensitivity limit of 0.2% . This amounts to a 54 percent detection rate to be compared with ∼58 percent here. These percentages are strikingly alike. The similarity in both spectropolarimetric behaviour and detection rate is a strong hint that Herbig Be stars are embedded in electron-scattering circumstellar discs of similar characteristics to those associated with classical Be stars. This allows the interpretation of the non-detections to be examples of Herbig stars with their discs too face-on to yield measurable line depolarisations.

The predominance of (Q, U) loops in the Herbig Ae star spectropolarimetry suggests that compact Hα emission that is itself scattered and polarised by a rotating, nonspherical medium is the norm. Prior examples of this spectropolarimetric behaviour and discussion of its origin may be found in studies of the peculiar Be star γ Cas (Poeckert & Marlborough 1977) and the Wolf-Rayet binary EZ CMa (Schulte-Ladbeck et al. 1990). That the frequency of effects among the Herbig Ae stars is possibly higher than among the Herbig Be stars might be expected as the PA rotation can remain visible over a wider range of viewing angles. In the case of AB Aur, Pontefract et al (2000) have suggested that the spectropolarimetric evidence of a rotating, flattened structure surrounding a compact Hα source might be due to magnetically-channelled accretion. Catala et al. (1999) also invoked this possibility in the face of a detection of time-variable redshifted absorption in HeI lines in

AB Aur. Our data include two instances of stars showing significant redshifted absorption at Hα (T Ori and CQ Tau), and many more instances of (Q, U) loops. (Note that infall features at Hα were previously found by e.g. Finkenzeller & Mundt 1984; de Winter et al. 1999). Independently, the two lines of evidence would not be such a strong indication of magnetically-channelled accretion – but together they are rather more compelling. To pursue this issue further, an interesting next step would be to compare the linear spectropolarimetric characteristics for the Herbig stars with those in the lower mass T Tauri stars, a class of young objects for which the magnetically-channelled accretion model is better established (Edwards et al. 1994; Hartmann 1999). So far only circular spectropolarimetry has been published (Johns-Krull, Valenti & Koresko 1999) for T Tauri stars.

We now consider why there is the observed difference between the Herbig Be and HAe groups, and what it might mean. One point of view could be that there is a physical transition region in the Hertzsprung-Russell Diagram where the geometry changes, as possibly the mode of presumed accretion changes. While the Herbig Ae stars might experience magnetically-channelled accretion resembling that associated with T Tauri stars, the Herbig Be star accretion flow may not be disrupted at a magnetospheric radius. The possibility that this might be so inspired the exploration of a radiation-driven disc wind concept for Herbig Be stars and embedded Becklin-Neugebauer objects presented by Drew, Proga & Stone (1998). Before the option of a real transition can be accepted it is important to recognise that the difference may instead simply be one of observational contrast.

Crudely speaking, spectral type maps onto effective temperature and, indeed, luminosity – if differences in evolutionary age are taken to be a secondary influence in our sample. Assuming all environmental factors such as the geometry and quantity of circumstellar matter around all Herbig Ae/Be stars to be the same, the mere facts of the higher temperatures and luminosities of the HBe stars imply greater extension of the ionised regions around them, and of course larger dust-free cavities. In accord with this, Hα equivalent width is indeed greater among the HBe stars than among the HAe stars. In the presence of reduced Hα line emission and opacity for the HAe stars it is easier to detect the interior component that we require should exist inside an axisymmetric rotating structure. The failure to detect this at Hα in the early Be stars could then be nothing more than a masking of it by the sheer size of the total line-emitting volume and its optical depth.

We have counted MWC 361 (see Fig. 4) as an instance of broad line depolarisation. This may not be the entire story. The data for this object show a relatively narrow PA rotation in the red wing of Hα, on top of what otherwise is a well-defined wide depolarisation. This may hint at some interior Hα polarisation reminiscent of that seen among the HAe stars. Significantly, perhaps, the Hα equivalent width measured for MWC 361 (-63Å) is lower than for most of the other early HBe stars showing simple depolarisations. A difficulty may however be presented by the case of MWC 166 (HD 53367). This early HBe star also has a relatively small Hα equivalent width (−2.8Å rather and −14Å in OD99), but no evidence of a compact Hα component. In other words, spectropolarimetrically it does not look like an HAe star. The counter to this is to argue that a reclassification of

this object is appropriate. Evidence to support this can be derived from the relative weakness of MWC 166's infrared continuum excess: Hillenbrand et al. (1992) classify it as a Class III source because it is so weak. These Class III objects are hard to distinguish from more mature classical Be stars. Perhaps MWC 361 is the seemingly peculiar case that ultimately betrays the geometric parallels between the environments of HAe and HBe stars. However, caution must be exercised in view of the potential impact of the known binarity of MWC 361 (Millan-Gabet, Schloerb & Traub 2001).

There is a test that might distinguish between the two options discussed above. Spectropolarimetry could be performed across less opaque, higher excitation emission lines that can be expected to arise in the same location as the compact Hα component, if it exists in the HBes. If the extension and optical depth of Hα emission indeed masks the evidence of a compact source in the HBes, e.g. He I or higher Balmer line observations could reveal angle rotations (Q, U loops) in both the HBe and the HAe stars. If however, angle rotations were not observed in the HBe population, while appearing among the HAe stars, then the balance of the argument would shift in favour of HBe environments being physically different from those of HAe stars on the smallest scales.

As we have found that flattened structures around Herbig Ae/Be stars are common in our data, we wonder how this compares with the existing literature on this matter. We have therefore checked if the spectropolarimetric behaviour of our HAe sample correlates at all with the so-called UXOr phenomenon (named after UX Ori). The UXOr phenomenon is believed, by some authors, to be associated with dusty clouds orbiting the young star in a close to edge-on disc-like structure (see e.g. Natta et al. 1997, but see Herbst & Shevchenko 1999 for a conflicting view). Six of the HAe stars from our sample appear in the HAe compilation by Natta et al., but only three of these undergo photometric changes larger than 1 mag in the V band characteristic for UXOrs[1]. As some of the stars that do not show UXOr behaviour do show loops in (Q, U) space, this indicates that the UXOr and spectropolarimetric behaviour have different physical origins: the UXOr behaviour may well be linked with large scale dusty clouds, while the spectropolarimetry yields insights on the structure of the accretion flow much closer to the star.

Recently, Millan-Gabet et al. (2001) conducted an interferometric study at near-infrared wavelengths and they concluded that accretion disc models can be ruled out in most cases. Instead it was claimed that spherical models reproduce the visibility data much better. Note the seeming contradiction with the findings of the spectropolarimetry. But what are the spatial scales involved? The Herbig Ae stars in Sect. 4.2 of this study show loops in (Q, U) space, associated with PA changes measured to be as narrow as $\sim$ 10 Å. This wavelength width translates into a velocity in the rotating disc of about 225 km s^{-1}. Assuming a stellar mass of $\sim$ 2 M$_\odot$, we find that this rotation speed corresponds to spatial scales of only $\sim$ 7 stellar radii, or equivalently 0.07

AU. This is to be compared to the scales of $0.5 - 5$ AU that the interferometry of Millan-Gabet et al. can resolve.

We conclude that the spectropolarimetry indeed probes the smallest-scale structures of the circumstellar medium, which are found to be flattened.

REFERENCES

Bjorkman K.S., Johansen K.A., Nordsieck K.H., Gallagher J.S., Barger A.J., 1994, ApJ 425, 247

Bonnell I.A., Bate M.R., Zinnecker H. 1998, MNRAS 298, 93

Bouvier J., Forestini M., Allain S., 1997, A&A 326, 1023

Cassinelli J.P., Nordsieck K.H., Murison M.A. 1987, ApJ 317, 290

Catala C., Donati J. F. Böhm T., et al., 1999, A&A 345, 884

Clarke D., McLean I.S. 1974, MNRAS 167, 27

Cropper M., Bailey J., McCowage J., Cannon R.D., Couch W.J., 1988, MNRAS 231, 695

Drew J.E., Proga D., Stone J.M. 1998, MNRAS 296, L6

Edwards S., Hartigan P., Ghandour L., Andrulis C., 1994, AJ 108, 1056

Finkenzeller U., Mundt R., 1984, A&AS 55, 109

Ghosh P., Lamb F. K., 1979, ApJ 232 259

Grinin V.P., 1994, in ASP Conf.Sers. No. 62 *The Nature and evolutionary status of Herbig Ae/Be stars*, eds. P.S. Thé , M.R. Pérez, E.P.J. van den Heuvel, p. 63

Grady C.A., Woodgate B., Bruhweiler F.C., et al., 1999, ApJ 523, L151

Harries T.J., Howarth I.D., 1996, A&A 310, 533

Hartmann L., 1999, NewAR 43, 1

Herbig G.H. 1960, ApJS 4, 337

Herbst W., Shevchenko V.S., 1999, AJ 118, 1043

Hillenbrand L.A., Strom S.E., Vrba F.J., Keene J. 1992, ApJ 397, 613

Jain S.K., Bhatt H.C., 1995, A&AS 111, 399

Johns-Krull C.M., Valenti J.A., Koresko C., 1999, ApJ 516, 900

Magalhães A.A. 1992, ApJ 398, 286

Mannings V., Sargent A.I., 1997, ApJ 490, 792

McLean I.S., 1979, MNRAS 186, 265

Millan-Gabet R., Schloerb F.P., Traub W.A., 2001, ApJ 546, 358

Natta A., Grinin V.P., Mannings V., Ungerechts H., 1997, ApJ 491, 885

Oudmaijer R.D., Proga D., Drew J.E., de Winter D., 1998, MNRAS 300, 170

Oudmaijer R.D., Drew J.E. 1999, MNRAS 305, 166

Oudmaijer R.D., Palacios J., Eiroa C., et al., 2001, A&A 379, 564

Petrova N.N., Shevchenko V.S., 1987, PAZh 13, 686

Pezzuto S., Strafella F., Lorenzetti D. 1997, ApJ 485, 290

Poeckert R. 1975, ApJ 152, 181

Poeckert R., Marlborough J.M., 1976, ApJ 206, 182

Poeckert R., Marlborough J.M., 1977, ApJ 218, 220

Pontefract M., Drew J.E., Harries T.J., Oudmaijer R.D., MNRAS 319, L19

Rudy, R.J., 1978, PASP 90, 688

[1] This is a very loose description of the UXOr behaviour. Strictly speaking, the star should undergo a colour reversal (blueing effect) which is characteristic for UX Ori itself

Schulte-Ladbeck R.E., Nordsieck K.H., Nook M.A., et al., 1990, ApJ 365, 19

Schulte-Ladbeck R.E., Clayton G.C., Hillier D.J., Harries T.J., Howarth I.A. 1994, ApJ 429, 846

Shepherd D.S., Claussen M.J., Kurtz S.E., 2001, Sci 292, 1513

Thé P.S., de Winter D., Perez M.R. 1994, A&AS 104, 315

Tinbergen J., Rutten R. 1997, 'Measuring polarization with ISIS'

Tody D. 1993, in ASP Conf. Series 52 *Astronomical Data Analysis Software and Systems II*, eds. R.J. Hanisch, R.J.V. Brissenden, J. Barnes, Astron. Soc. Pac., San Francisco, p. 173.

Vrba F.J., Schmidt G.D., Hintzen P.M., 1979, ApJ 227, 185

Waters L.B.F.M., Marlborough J.M., 1992, A&A 265, 195

Waters L.B.F.M., Waelkens C., 1998, ARAA 36, 233

Wood K., Brown J.C., Fox G.K., 1993, A&A 271, 492

Yorke H.W., Kruegel E., 1977, A&A 54, 183

Zickgraf F.-J., Schulte-Ladbeck R.E., 1989, A&A 214, 274